RSC Advances

ROYAL SOCIETY OF CHEMISTRY

www.rsc.org/advances

Journal Name

RSCPublishing

ARTICLE

"Unrolling" Multi-walled Carbon Nanotubes with Ionic Liquids: Application as Fillers in Epoxy-Based Nanocomposites

Cite this: DOI: 10.1039/xoxxoooooox

Received ooth January 2012,
Accepted ooth January 2012

DOI: 10.1039/xoxxoooooox

www.rsc.org/

A.C. Kleinschmidt,[1,2] R. K. Donato,[2*] M. Perchacz,[3] H. Beneš,[3] V. Štengl,[4] S. C. Amico,[1] H. S. Schrekker[2*]

This work describes a straightforward procedure for the preparation of graphene by opening multi-walled carbon nanotubes (CNT), using ionic liquids (IL) as lubricating and stabilizing agents. The sequential application of vacuum and sonication allows the successful CNT opening and unrolling, and the final nanocarbon morphology is IL-dependent. This enabled the preparation of epoxy-based nanocomposites with morphologically distinct carbon nanofillers. The CNT-IL mixtures and nanocomposites obtained were characterized by transmission electron microscopy (TEM), scanning electron microscopy (SEM), atomic force microscopy (AFM) and Raman spectroscopy.

Introduction

The beginning of research and development of carbon-based nanomaterials (CNM), as for the fullerene, was around the 1980's.[1] Thenceforth, a variety of different carbon allotropes were discovered and these are usually classified by their geometry,[1,2] e.g.; fullerenes (0-D), carbon nanotubes or nanofibers (1-D), graphene sheets (2-D) and graphite (3-D). In fact, CNM have been used for centuries, however the rational use of their properties is only nowadays in its infancy.[3] One of the main motivations on learning about the manipulation of these materials is their peculiar characteristic of bestowing dramatic property changes, i.e.; electrical, mechanical, thermal, with minimum carbon application.[4]

Within this class of materials, carbon nanotubes (CNT) were discovered only in 1991 in its Matrioshka doll shape (formed by several concentric tubes) or as bundles (rolled graphene sheets),[5] and in 1993 the application of catalysts allowed the formation of CNT constituted of a single wall.[6,7] Interestingly, although being known since the 1940's, graphene (a bidimensional layer of sp^2 carbons)[1] was considered as an "unrealistic" material due to its production hurdles and low thermodynamic stability at ambient conditions. In 2004, the work of Geim and Novoselov changed this perspective, showing that graphene was not only a "possible" material but also accessible, if alternative approaches would be applied for its obtention.[4,8,9] Thereafter, the production and use of graphene became of strategic interest, representing a promise of breakthroughs for several areas, especially materials sciences. Despite of such blaze caused by the advances in this area and the relative abundance of prime material for its formation, the road to reach the production of graphene based materials as a commodity is still long.[10]

The biggest challenges for obtaining and using graphene are the low efficiency of the available methods. Several top-down and bottom-up methods have been demonstrated in the literature, but still a good balance among productivity, quality and cost is a goal to be reached.[4,10] A feasible option for obtaining graphene nanoribbons with regular sizes is through "unzipping" or "unrolling" of CNT,[11-14] but mostly these procedures use a method commonly applied for graphene preparation that involves an aggressive oxidation, creating dispersed graphene oxide (GO) sheets or ribbons (Hummer method).[15] Herein, the major drawback is the use of strong acids (H_2SO_4, HNO_3) and oxidizing agents ($KMnO_4$, CrO_3) for GO formation, which is than exposed to strong reducing agents ($NaBH_4$), hydrazine vapour or hydrogen at high temperatures (600 – 800 °C). The inconveniences of this process, together with the formation of oxidation debris, disable it for large-scale production.[16]

The search for milder conditions and higher graphene yields led to several procedures,[11,14,17,18] among which the irradiation of graphite or CNT dispersions in solvents and/or surfactants presented significant results.[19-21] The main parameter for a successful exfoliation is in the properties of the solvents/surfactants used, which need to provide enough solvent/surfactant-graphene interaction for the expansion of the graphene layers.[22] However, generally the mentioned

procedures involve the usage of volatile organic solvents, which present problematic environmental issues as well as technological inconvenience regarding the potential application of graphene for nanocomposite preparations.

Recently, the application of ionic liquids (IL) has been showing promising results on structural control of nanocomposites.[23,24] IL are organic salts with low melting points; often they are liquid at room temperature and present several intrinsic properties, e.g., low volatility, high thermal and chemical stability, insignificant flammability, good thermal conductivity, high ionic mobility and moisture resistance.[25-27] The imidazolium-based IL present these properties together with the strong capacity of interacting with carbon based materials. A "π-π stacking" of the IL cations at the π-electronic surface of the sp^2 carbon network allows it to act as both solvent and surfactant due to the IL's amphiphilic structure.[28] These features make IL ideal for exfoliating/stabilizing graphene through a solution irradiation process, allowing broader experimental conditions, as soon as volatile organic solvents have the drawback of limited working temperature ranges.

In this work we present a mild process (relatively low energy irradiations and temperatures) to prepare high quality, oxidative debris free, graphene nanoribbons and sheets from unrolling multiwalled carbon nanotubes (MWCNT) in IL media, which were used to prepare reinforced epoxy-graphene nanocomposites with minimum filler content (~0.1 wt.-%). Vadahanambi *et al.* reported about the use of an IL-assisted splitting method under microwave radiation for the production of graphene nano-ribbons from multi-wall or single wall carbon nanotubes.[29] Differently from our approach, this method is based on the decomposition of the BF_4 IL anion, using the generated fluorine as the "splitting agent" for the CNT. The main differences between the two processes are the radiation source (microwave vs. ultrasound) and the nature of the process itself (chemical vs. physical modification). The NTf_2 IL anion used in our process is thermally and chemically much more stable, allowing graphene formation and stabilization without decomposition of neither CNT nor IL.

Experimental

Graphene formation by CNT opening

Multi-walled CNT with 140 nm of diameter and average length of 7 μm (Strem Chemicals Inc., purity >90%) were mixed with the IL 1-*n*-butyl-3-methylimidazolium bis(trifluoromethane-sulfonyl)imide ($C_4MImNTf_2$; Sigma-Aldrich, purity ≥98%) or 1-*n*-butyl-3-methylimidazolium chloride (C_4MImCl; Sigma-Aldrich, purity ≥98%) under vacuum at different cycles of mechanical and ultrasonic stirring (Sonics VCX 750 W working at 185.5 W, f = 20 kHz). The same process was applied in the presence of toluene as a comparison for the process with IL. As a manner of limiting the cost of this process, the CNT were applied as received, without removal of amorphous carbon or other treatment of any sort.

Four different routes were defined, varying heating time, stirring under vacuum and sonication time of the CNT-IL (1:10 mass ratio) mixtures. The routes were organized in a way to observe gradually the relation between energy applied and efficiency of CNT unrolling, as well as individual contribution of temperature, mechanical stirring and ultrasound application: a) 1 h of heating (100 °C) and mechanical stirring under vacuum, followed by 90 min of ultrasound application at room temperature; b) 1 h of heating and mechanical stirring under vacuum, followed by 3 h of ultrasound application at room temperature; c) 3 h of heating and mechanical stirring under vacuum, followed by 90 min of ultrasound application at room temperature; d) 3 h of heating and mechanical stirring under vacuum, followed by 3 h of ultrasound application at room temperature. All the procedures were divided in 3 cycle for each part, i.e, a 3 h heating/vacuum followed by 3 h sonication means 3 cycles of 1 h heating/vacuum followed by 3 cycles of 1 h sonication.

CNT/graphene-epoxy nanocomposites formation

The previously obtained treated CNT were mixed at 60 ºC under vacuum for 1 h with a Diglycidylether of Bisphenol A based epoxy resin (Araldite LY1316, Huntsman). Then, the mixtures were put under ultrasonic stirring (247.5 W) during 30 min, followed by the addition of 13 wt.-% of the triethylenetetramine hardener (Aradur HY951). The mixtures were then poured into silicone molds and left for curing for 24 h to produce specimens via casting. The specimens were submitted to post-curing under vacuum for 1 h at 130 ºC.

Characterization

Transmission electron microscopy (TEM): TEM was realized using 2 standard TEM microscopes (JEOL JEM 1200 ExII and Carl Zeiss Libra 120) both under tension of 80 kV with electron thermo-ionic emission of tungsten filament. Two kinds of samples were studied: (i) neat CNT/graphene dispersed in IL and (ii) epoxy/graphene nanocomposites. (i) For characterizing the CNT/graphene – IL dispersions, a 2 μL droplet of the suspension in ethanol was transferred to a microscopic carbon-coated copper grid, the excess of the liquid was gently removed with a filtration paper and the grid was left to equilibrate at room temperature. (ii) As for nanocomposites containing CNT/graphene dispersed in the epoxy matrix, the specimens were ultramicrotomed (with an ultramicrotome RMC Power Tome XL) in order to obtain ultrathin sections (~40 nm); the sections were transferred to the TEM 300 mesh copper grids.

Atomic Force Microscopy (AFM): AFM images were obtained using a Bruker Dimension ICON FastScan microscope. Specimens were prepared by a spin-coating method that consisted of pipetting an aqueous suspension of CNT-IL samples onto an atomically smooth support of synthetic mica. The suspension was spin coated on the mica substrate at 6000 rpm. A silicon tip on a nitride lever was used with ScanAsyst - air contact mode (resonance frequencies 50 / 90 kHz).

Scanning Electron Microscopy (SEM): SEM images were obtained from the fractured surface of specimens submitted to the IZOD impact test. The surfaces were gold coated and analyzed using 20 kV electron beams in a Jeol JSM 6060 microscope.

Raman Spectroscopy: The IL-CNT mixtures were characterized by Raman spectroscopy in a Labram – JobinYvon/Horiba Raman spectrometer with He/Ne laser with $\lambda = 632.8$ nm, 0.5 mW of power, under a 200 s acquisition time.

Results and discussion

CNT "unrolling" to graphene

Initially, a study was realized to define the most efficient procedure for opening and unrolling the CNT using the IL media for dispersion and stabilization (presented in the experimental part). As the event of CNT opening consists of a drastic morphological change, after applying the different procedures, microscopic analysis was used for qualitative evaluation of the method (**Fig. 1**). When the CNT-C_4MImNTf_2 mixtures were exposed to temperature and ultrasound treatments for short periods the initial structure of CNT seems unaltered (**Fig. 1a**). With increasing the temperature exposition, the beginning of the CNT opening process can be observed (**Fig. 1c**), but clearly the increase of exposition to ultrasound produces a much more significant effect (**Fig. 1b**). Increasing both the temperature/vacuum and ultrasound exposition an almost complete CNT opening is observed (**Fig. 1d**). In general, when applied higher temperature (150 ˚C) apparent thermo-oxidative processes were observed. Based on these findings, the procedure of 3h mechanical stirring under vacuum at 100 ˚C followed by 3h of ultrasound was chosen as standard for further studies, as it allows a good efficiency on CNT opening without apparent damage by thermal decomposition.

The fundamental importance of the IL in this process is evidenced by comparing the TEM images of the original CNT (**Fig. 1e**) with the ones from a CNT-toluene mixture (**Fig. 1f**) and CNT-C_4MImNTf_2 (**Fig. 1d**), both applied to the optimized procedure.

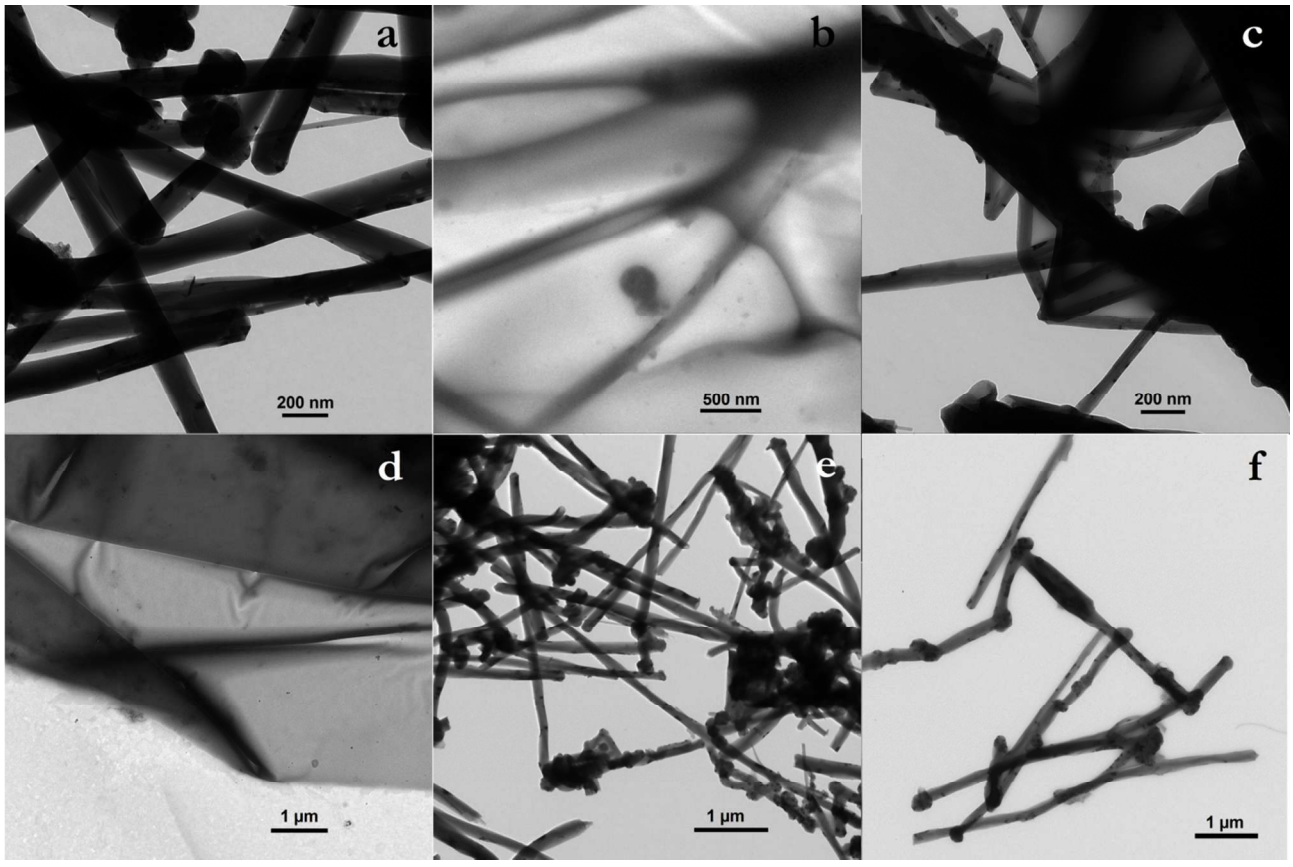

Fig. 1 TEM images of CNT-C_4MImNTf_2 mixtures applying different mechanical and ultrasound stirring regimens; a) 1 h of heating-mechanical stirring and 90 min of ultrasound stirring; b) 1 h of heating-mechanical stirring and 3 h of ultrasound stirring; c) 3 h of heating-mechanical stirring and 90 min of ultrasound stirring; d) 3 h of heating-mechanical stirring and 3 h of ultrasound stirring; also the images of e) original CNT and f) CNT-toluene mixture used as references.

Toluene was used due to its electronic resemblance with the CNT surface, which could promote the disruption of the π-packing from the CNT bundles. Nevertheless, the CNT-toluene mixture presents no structural difference with the original CNT, despite some partially swelled superficial layers and smaller bundle sizes due to the effect of dilution (**Fig. 1e vs. 1f**). This evidences the unique role of the IL in CNT unrolling (**Fig. 1e vs. 1d**).

In an attempt to elucidate the process through which the CNT loses its original structure, AFM images of CNT in different unrolling stages were taken. Apparently, a process of CNT swelling-unrolling is taking place during sonication in IL media. The pristine CNT presents a diameter of ~150 nm (**Fig. 2a**). Initially the CNT swells more than twice its diameter (~ 400 nm), which forces it to lose the layered structure of the inner walls and an unrolling process is started (**Fig. 2b**). This swelling could be the result of IL penetration among the CNT walls during the sonication process, leading to the formation of cavitation in the CNT and producing enough energy to separate the previously π-packed graphene layers. As a result of this process, micrometric-sized tactoids consisting of few layered graphene sheets (~ 15 nm thick) are formed (**Fig. 2c and 2d**).

Although the CNT-IL interactions are mainly governed by the π-π packing between sp^2 carbons from CNT and the IL imidazolium ring,[28] the IL anion size and polarity play important roles in the IL permeation among the highly compacted CNT walls as well. This phenomenon of CNT unrolling is influenced by the composition of the IL anion, as a matter of increasing the CNT-IL interaction by polarity tuning, however, and the IL anion size appears to be crucial.

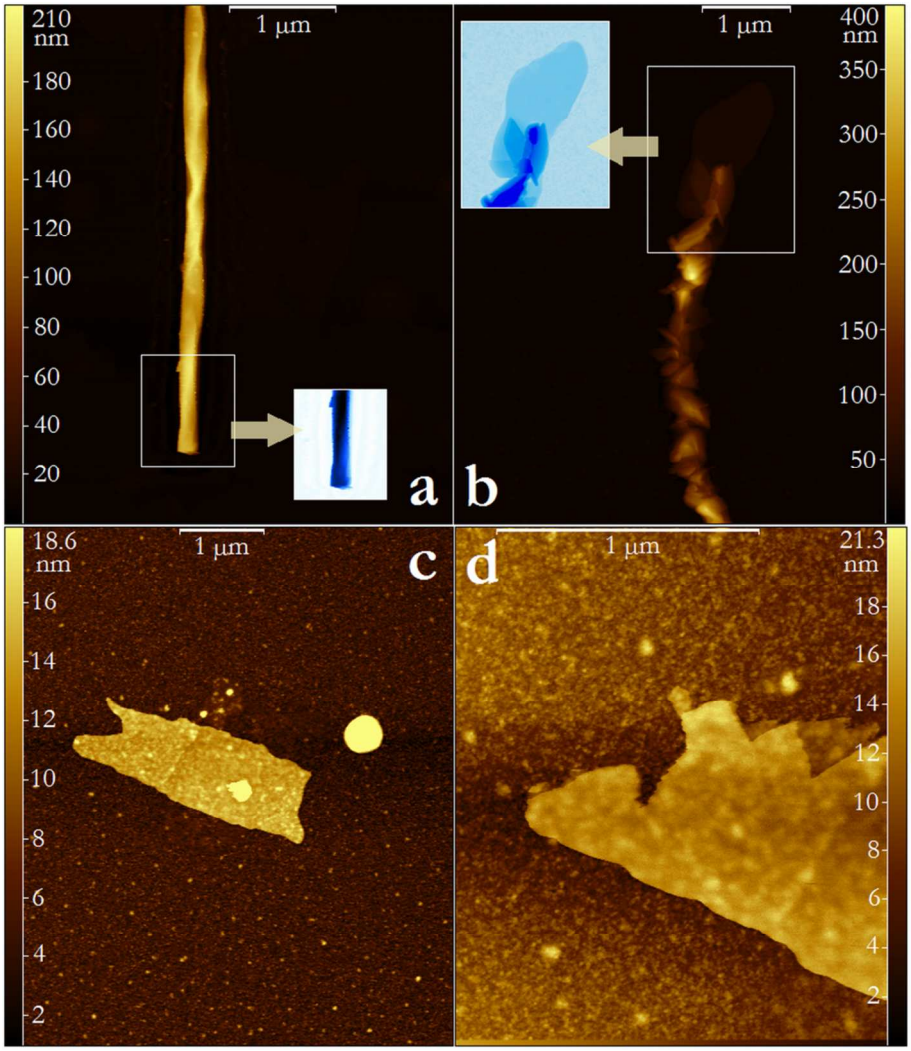

Fig. 2 AFM images of; (a) untreated CNT, showing in the detail a compact and unaltered extremity; (b) swelled and partially unrolled CNT, showing in the detail the graphene sheets disconnecting from the main axial structure; (c) completely unrolled micrometric graphene sheet; (d) the edge of an unrolled layered graphene tactoid.

Once the molecule vibrates under the ultrasonic influence, larger molecules will form a larger momentum, producing a larger number of cavitation bubbles.[30] When $C_4MImNTf_2$ is applied, where NTf_2^- is a large and hydrophobic anion, CNT opening is clearly observed (**Fig. 1d**). Differently, when using the chloride anion equivalent C_4MImCl in this process, no CNT unrolling can be observed (**Fig. 3a**). Despite this observation, C_4MImCl appears to be efficiently disentangling the CNT bundles to only small aggregates, functioning in this case as a type of dispersing-lubricating agent. Such a mechanism of CNT isolation from a bundle using sonication and surfactant (non-covalent) adsorption was previously mentioned in the literature.[31] Firstly, the ultrasonic treatment provides high local shear to the CNT bundle-end, which leads to the formation of larger spaces among CNTs. Subsequent surfactant adsorption further enlarges the CNT distances and results into the

separation of the individual CNTs from its bundle. It has been proved that π-stacking interactions of the benzene rings (or other highly aromatic molecules) onto the CNT surface increase the adsorption ratio of surfactants.[32-34] Similarly in our case, the imidazolium ring of C_4MImCl interacts with the CNT surface via π-π electron bonding, which promotes its surfactant effect and dispersion strength. The presence of C_4MImCl as supramolecular aggregates all over the CNT surface can be observed, as dark spots, in **Fig. 3b**.

The quality of CNM is widely characterized by Raman Spectroscopy, providing information especially about the tangential G band derived from the in-plane vibration of the sp^2 carbon atoms and the disorder-induced D band.[11,35,36] The ratio of the D to G band intensities (I_D/I_G) is related to the density of defects and edge smoothness of the graphene.[37]

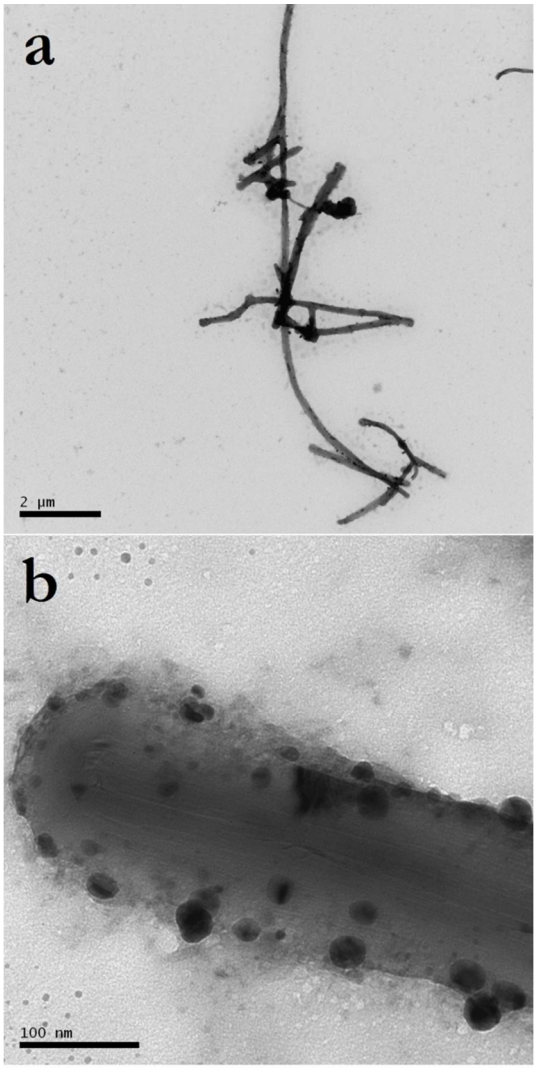

Fig. 3 TEM images of the CNT-C_4MImCl mixture; a) scale bar = 2 µm and b) scale bar = 100 nm.

The I_D/I_G ratio of the CNT-C_4MImNTf$_2$ mixture is ~ 0.2, much lower than the ones presented by GO layers unzipped from CNT by the solution-phase oxidation (I_D/I_G > 1)[12] or by mechanical sonication (I_D/I_G ~ 0.4),[19] which indicates the high quality of the graphene layers unrolled from the CNT using IL. Despite the good values for the I_D/I_G ratio, a drawback on the use of Raman spectroscopy of IL-CNM mixtures is the overlap of the D band from the CNM (**Fig. 4a**) with the Raman active bands of the imidazolium cation (**Fig. 4b** and **c**).[38] This means that the values for the D band could be even lower, consequently affecting the I_D/I_G ratio and representing a false positive for CNT/graphene defects. This effect is not so evident in the CNT-C_4MImNTf$_2$ mixture, where the D band is quite small in relation to the G band (**Fig. 4b**), but for the CNT-C_4MImCl mixture it turns to be completely unreliable as the most prominent band is the one from the IL cation (**Fig. 4c**). Such a difference between the two applied IL is a probable consequence of the less homogeneous distribution of C_4MImCl over the CNT surface, as observed (**Fig. 3b**).

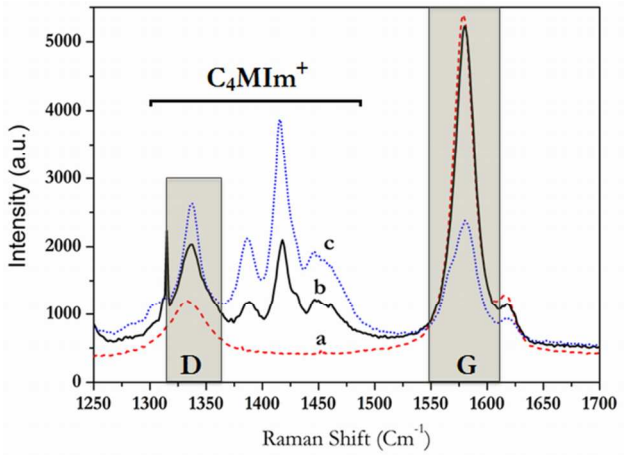

Fig. 4 Raman spectra of a) original CNT, b) CNT-C_4MImNTf$_2$ mixture and c) CNT-C_4MImCl mixture. The highlighted areas identify the G and D band positions. The bar is delimitating the region with Raman active bands from the IL cation.

3.2 Formation of epoxy-CNT/graphene nanocomposites

The prepared CNT/graphene mixtures were applied as filler in the epoxy resin synthesis process to evaluate the IL's capacity of stabilizing the CNM during the polymer network formation. This process involved an amine (triethylene tetramine) hardened epoxy polyaddition reaction to form a highly cross-linked network. The most crucial point for this process was to evaluate if the IL are able of avoiding the unrolled CNT to re-agglomerate or even form higher hierarchically packed bundles or tactoids. TEM micrographs show structural differences among CNT-epoxy, CNT-C_4MImCl-epoxy and CNT-C_4MImNTf$_2$-epoxy nanocomposite systems (**Fig. 5**). When the original CNT was mechanically and ultrasonically stirred directly with the epoxy polycondensation precursors, well defined CNT were observed (**Fig. 5a**). Substituting pristine CNT by the CNT-C_4MImCl mixture didn't cause a significant effect on the tubular structure, with the exception of a small swelling effect at the tips of CNT (**Fig. 5b**). This was also observed for the pristine CNT nanocomposite as a result of damaging during the specimen production by ultramicrotomy, as the CNT chosen are fairly long. The same process applied to

the CNT-C_4MImNTf_2 mixture caused a drastic morphological change, with the apparent CNT opening and stabilization in small tactoids of few graphene sheets (**Fig. 5c**) or ribbons (**Fig. 5d**).

TEM images collected from these nanocomposites allowed observing the different stages of CNT opening, with the presence of C_4MImNTf_2, until forming completely unrolled graphene sheets or tactoids (**Fig. 6**). The apparent mechanism corresponds to unrolling of graphene sheets from a parallel axis. Initially a highly packed and electron dense CNT structure is observed (**Fig. 6a**). With temperature and application of ultrasound this structure's outer layers eventually swell and unglue from the main axis (**Fig. 6b** and **c**), followed by the complete disconnection of the sheet from the main axis (**Fig. 6d**) and formation of the graphene domains (**Fig. 6e**), which corroborates with the previously displayed AFM results.

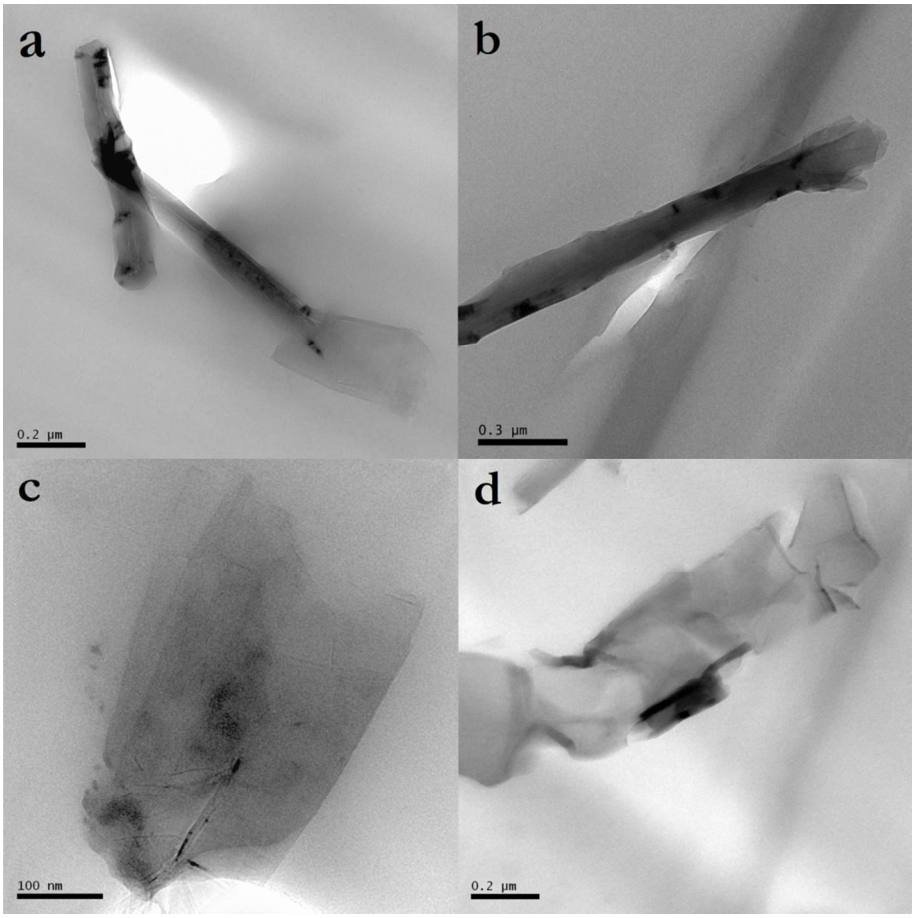

Fig. 5 TEM images of the nanocomposites based on a) CNT-epoxy without IL, b) CNT-C_4MImCl-epoxy and c-d) CNT-C_4MimNTf_2-epoxy systems.

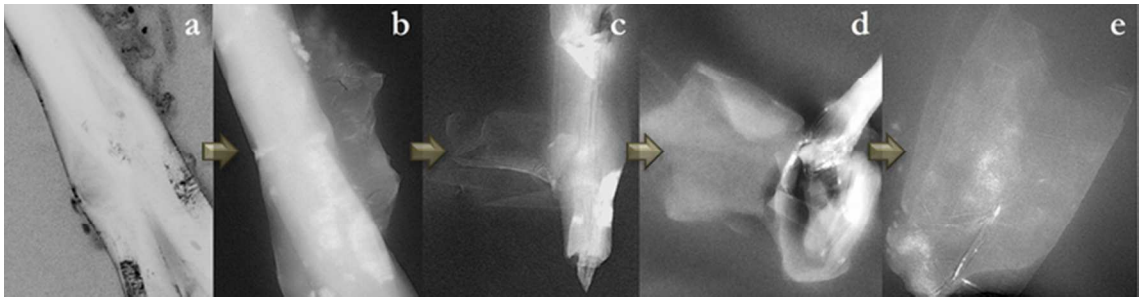

Fig. 6 TEM images of the CNT opening process in the presence of IL C_4MImNTf_2; a-b) initial CNT swelling-unrolling, c-d) "unpacking" of the outer graphene layers and e) fully opened layered graphene. The images are presented in negative as a matter of increasing the contrast between background and the electron dense objects.

Evaluating the size of the final graphene sheets formed, it is clear that this material was ripped at some point of the process. Comparing **Fig. 1** and **2** vs. **Fig. 5**, the final fillers formed are from different orders of magnitude. Most likely, two different

events could explain this increase in filler-size: i) filler ripping during the network formation process; and ii) filler ripping during the nanocomposite ultramicrotomy procedure for TEM specimen preparation (as also evidenced by the CNT tip rupture). To investigate these two possibilities, the nanocomposites were submitted to cryogenic fracturing and SEM evaluated their fractured regions. This method was chosen due to the filler exposition at the fracture surface, revealing the real structure of the final fillers formed and eliminating the ultramicrotomy step from TEM analysis.

Figure 7a presents the relatively smooth and filler free surface of the neat epoxy matrix, which was used as a reference. The IL free epoxy-CNT nanocomposite presented a similar surface fracture structure, but with the presence of randomly dispersed CNT (**Fig. 7b**), indicating the low CNT-epoxy interaction. The CNT-epoxy nanocomposite containing IL C_4MImCl presents a quite different fracture structure, exposing epoxy-coated CNT structures at the surface (**Fig. 7c**).

This could be a result of local plasticization of the epoxy network, avoiding the brittle break at the epoxy-CNT interphase, as this sample presents IL aggregation at the CNT surface (**Fig. 3b**). In the case of the epoxy-CNT nanocomposite with CNT-C_4MImNTf_2, it's fracturing changed drastically. This nanocomposite presents fractures in the shape of sheets, suggesting an epoxy-graphene interface fracture (**Fig. 7d**). Furthermore, also unopened CNT were identified in this nanocomposite, indicating that the CNT opening process was not quantitative.

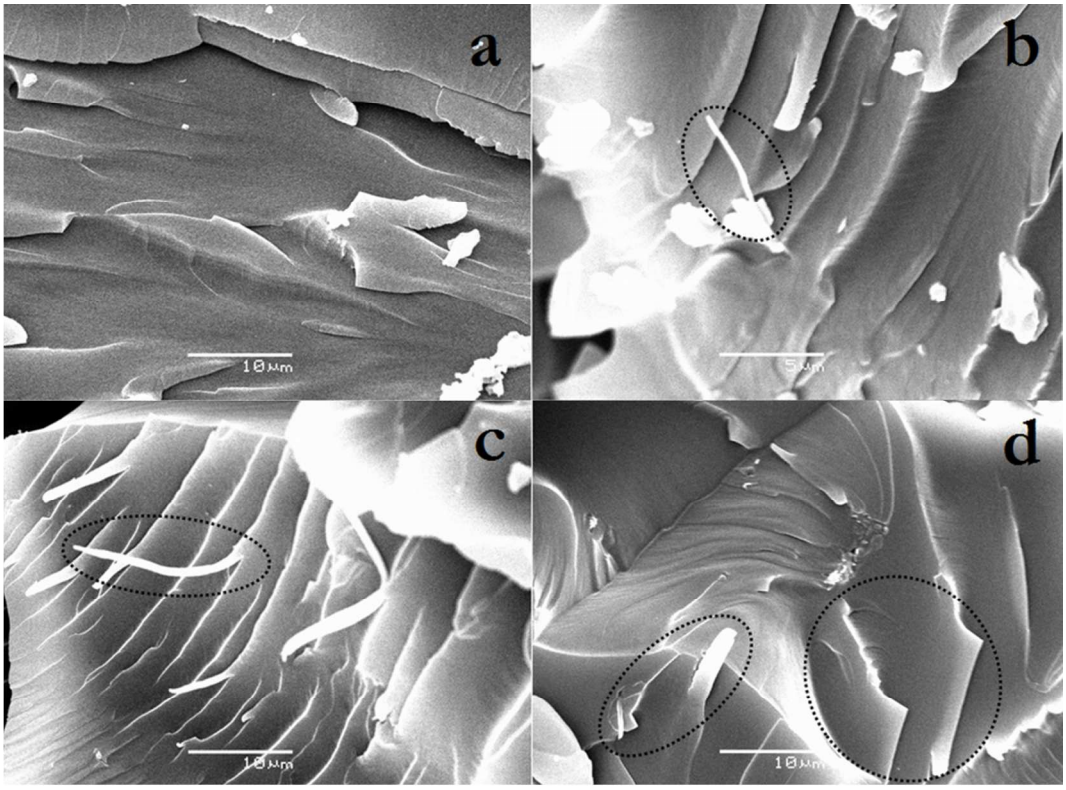

Fig. 7 SEM images of a) neat epoxy matrix (DGEBA-ethylene tetramine) and nanocomposites b) epoxy-CNT without IL, c) epoxy-CNT with IL C_4MImCl and d) epoxy-CNT with IL C_4MImNTf_2.

The detailed characterization and discussion of the thermo-mechanical properties, together with the influence of the different CNM morphologies and CNM-epoxy interfaces on the nanocomposite properties, will be the subject of our next paper.

Conclusions

A new route for the preparation of graphene sheets from multi-walled CNT was investigated, using suitable IL for the nanotube unrolling under ultrasound. It was found that the imidazolium-based cationic ring of IL exhibits a strong interaction with the CNT surface via π-π electron bonding. Nevertheless, the size and polarity of the IL anion has proven to be a crucial factor for successful CNT unrolling. During the ultrasound application, the CNT opening happened when the large and hydrophobic anion NTf_2^- was applied, which resulted in the formation of micrometric-sized tactoids consisting of few layered graphene sheets. On the other hand, the chloride anion did not have a tendency to penetrate into the CNT and open the π-packed graphene layers. Although this method still does not provide a very high CNT to graphene conversion yield, it is a promising strategy to obtain highly pure CNM structures under mild, non-oxidative and easy handling conditions, and allows the preparation of epoxy based CNM nanocomposites. A more detailed study about the process conditions is still in progress.

Acknowledgement

The authors are grateful to the Brazilian agencies CAPES, CNPq and FAPERGS for financial support. R. K. Donato is thankful to FAPERGS-CAPES for the DOCFIX post-doctoral fellowship. Financial support of the Grant Agency of the Czech Republic (project 14-05146S) is gratefully appreciated by M. Perchacz, H. Beneš and V. Štengl.

Notes and references

[a] Composite Materials Group - GCOMP, Polymer Materials Laboratory - LAPOL, Universidade Federal do Rio Grande do Sul - UFRGS - Porto Alegre-RS, Brazil.
[b] Laboratory of Technological Processes and Catalysis - Tecnocat, Institute of Chemistry, Universidade Federal do Rio Grande do Sul - UFRGS - Porto Alegre-RS, Brazil.
[c] Department of Polymer Processing - Institute of Macromolecular Chemistry - IMC, AS CR v.v.i. Prague, Czech Republic.
[d] Department of Solid State Chemistry, Institute of Inorganic Chemistry, AS CR v.v.i., Prague, Czech Republic.

1. M. Terrones, A. R. Botello-Mendez, J. Campos-Delgado, F. López-Urías, Y. I. Vega-Cantú, F. J. Rodríguez-Macias, A. L. Elías, E. Munõz-Sandoval, A. G. Cano-Márquez, J. C. Charlier, H. Terrones, *Nano Today*, 2010, **5**, 351.
2. H. Kim, A. A. Abdala, C. W. Macosko, *Macromolecules*, 2010, **43**, 6515.
3. C. Soldano, A. Mahmood, E. Dujardin, *Carbon*, 2010, **48**, 2127.
4. A. K. Geim, *Science*, 2009, **324**, 1530.
5. R. H. Baughman, A. A. Zakhidov, W. A. Heer, *Science*, 2002, **297**, 787.
6. P. Avouris, *IEEE Spectrum*, 2004, 41.
7. A. Maffucci, G. Miano, F. Villone, W. Zamboni, *IEEE Transaction on Magnetics*, 2008, **44**, 1614.
8. K. S. Novoselov, A. K. Geim, S. V. Morozov, D. Jiang, Y. Zhang, S. V. Dubonos, I. V. Grigorieva, A. A. Firsov, *Science*, 2004, **306**, 666.
9. A. K. Geim, K. S. Novoselov, *Nature Mater.*, 2007, **6**, 183.
10. C. K. Chua, M. Pumera, *Chem. Soc. Rev.*, 2013, **42**, 3222.
11. L. Jiao, L. Zhang, X. Wang, G. Diankov, H. Dai, *Nature*, 2009, **458**, 877.
12. D. V. Kosynkin, A. L. Higginbotham, A. Sinitskii, J. R. Lomeda, A. Dimiev, B. K. Price, J. M. Tour, *Nature*, 2009, **459**, 872.
13. Q. Liu, T. Fujigaya, N. Nakashima, *Carbon*, 2012, **50**, 5421.
14. S. Mohammadi, Z. Kolahdouz, S. Darbari, S. Mohajerzadeh, N. Masoumi, *Carbon*, 2013, **52**, 451.
15. W. S. Hummers, R. E. Offerman, *J. Am. Chem. Soc.*, 1958, **80**, 1339.
16. J. P. Rourke, P. A. Pandey, J. J. Moore, M. Bates, I. A. Kinloch, R. J. Young, N. R. Wilson, *Angew. Chem. Int. Ed.*, 2011, **50**, 3173.
17. B. Genorio, W. Lu, A. M. Dimiev, Y. Zhu, A.-R. O. Raji, B. Novosel, L. B. Alemany, J. M. Tour, *ACS Nano*, 2012, **6**, 4231.
18. D. B. Shinde, J. Debgupta, A. Kushwaha, M. Aslam, V. K. Pillai, *J. Am. Chem. Soc.*, 2011, **133**, 4168.
19. L. Jiao, X. Wang, G. Diankov, H. Wang, H. Dai, *Nature Nanotechnol.*, 2010, **5**, 321.
20. Y. Hernandez, V. Nicolasi, M. Lotya, F. M. Blighe, Z. Y. Sun, S. De, I. T. McGovern, B. Holland, M. Byrne, Y. K. Gun´ko, J. J. Boland, P. Niraj, G. Duesberg, S. Krishnamurthy, R. Goodhue, J. Hutchison, V. Scardaci, A. C. Ferrari, J. N. Coleman, *Nat. Nanotechnol.*, 2008, **3**, 563.
21. A. A. Green, M. C. Hersam, *Nano Lett.*, 2009, **9**, 4031.
22. A. B. Bourlinos, V. Georgakilas, R. Zboril, T. A. Steriotis, A. K. Stubos, *Small*, 2009, **5**, 1841.
23. R. K. Donato, K. Z. Donato, H. S. Schrekker, L. Matejka, *J. Mater. Chem.*, 2012, **22**, 9939.
24. R. K. Donato, L. Matejka, H. S. Schrekker, J. Plestil, A. Jigounov, J. Brus, M. Slouf, *J. Mater. Chem.*, 2011, **21**, 13801.
25. T. Welton, *Chem. Rev.*, 1999, **99**, 2071.
26. J. Dupont, R. F. de Souza, P. A. Z. Suarez, *Chem. Rev.*, 2002, **102**, 3667.
27. R. D. Rogers, *Nature*, 2007, **447**, 917.
28. T. Fukushima, T. Aida, *Chem. Eur. J.*, 2007, **13**, 5048.
29. S. Vadahanambi, J.-H. Jung, R. Kumar, H.-J. Kim, I.-K. Oh, *Carbon* 2013, **53**, 391.
30. T. J. Mason, *Sonochemistry*, Oxford Chemistry Primers, 2000, Oxford, UK.
31. M. S. Strano, V. C. Moore, M. K. Miller, M. J. Allen, E. H. Haroz, C. Kittrell, R. H. Hauge, R. E. Smalley, *J. Nanosci. Nanotech.* 2003, **3**, 81.
32. M. F. Islam, E. Rojas, D. M. Bergey, A. T. Johnson, A. G. Yodh, *Nano Lett*., 2003, **3**, 269.
33. L. Vaisman, H. D. Wagner, G. Marom, *Adv. Colloid Interf. Sci.*, 2006, **128**–**130**, 37.
34. R. Rastogi, R. Kaushal, S. K. Tripathi, A. L. Sharma, I. Kaur, L. M. Bharadwaj, *J. Colloid Interf. Sci.* 2008, **328**, 421.
35. Q. F. Liu, W. C. Ren, Z. G. Chen, D. W. Wang, B. L. Liu, B. Yu, F. Li, H. Cong, H.-M. Cheng, *ACS Nano*, 2008, **2**, 1722.
36. I. Calizo, A. A. Balandin, W. Bao, F. Miao, C. N. Lau, *Nano Lett.*, 2007, **7**, 2645.
37. C. Casiraghi, A. Hartschuh, H. Qian, S. Piscanec, C. Georgi, A. Fasoli, K. S. Novoselov, D. M. Basko, A. C. Ferrari, *Nano Lett.*, 2009, **9**, 1433.
38. T. Schafer, R. E. Di Paolo, R. Franco, J. G. Crespo, *Chem. Commun.*, 2005, 2594.

